

MODELLING AND SIMULATION OF TELECOMMUNICATION NETWORKS: ANALYSIS OF MEAN SHORTEST PATH LENGTHS

CATHERINE GLOAGUEN*, FRANK FLEISCHER**, HENDRIK SCHMIDT***,
VOLKER SCHMIDT***

*France Télécom R&D RESA/NET/NSO 92131 Issy les Moulineaux Cedex 9, France (catherine.gloaguen@francetelecom.com), **Department of Applied Information Processing and Department of Stochastics, University of Ulm, 89069 Ulm, Germany (frank.fleischer@uni-ulm.de), ***Department of Stochastics, University of Ulm, 89069 Ulm, Germany ({hendrik.schmidt,volker.schmidt}@uni-ulm.de)

Abstract. We consider random geometric models for telecommunication access networks and analyse their serving zones which can be given, for example, by a class of so-called Cox–Voronoi tessellations (CVTs). Such CVTs are constructed with respect to locations of network components, the nuclei of their induced cells, which are scattered randomly along lines induced by a Poisson line process. In particular, we consider two levels of network components and investigate these hierarchical models with respect to mean shortest path length and mean subscriber line length, respectively. We explain point–process techniques that allow for these characteristics to be computed without simulating the locations of lower–level components. We sustain our results by numerical examples which were obtained through Monte Carlo simulations, where we used simulation algorithms for typical Cox–Voronoi cells derived in a previous paper.

Keywords: telecommunication network modelling, stochastic geometry, point process, Palm probability, Neveu’s exchange formula, spatial tessellation, typical Cox–Voronoi cell, access network, shortest path, subscriber line

1 Introduction

Spatial stochastic models have been developed in recent years as alternatives to more traditional economical approaches for cost measurement and strategic planning of telecommunication networks; see, for example, [1], [2], [3], [4], [5], [6], and [14]. These models incorporate both stochastic as well as geometric features observable in telecommunication networks. While the random setting reflects the network’s variability in time and space, consideration of geometric structures of network architectures offer a more realistic view to location-dependent network characteristics than conventional models.

The access network or local loop is the part of the network connecting a subscriber to its corresponding Wire Center Stations (WCS), i.e. the place where the telecommunication network fits into the town and country infrastructure. The hierarchical physical link is made via network components. To each WCS we associate a serving zone such that the inscribed subnetwork that gathers all lines between the WCS and the subscribers displays a tree structure.

In recent years, access networks were studied in the context of the so-called Stochastic Subscriber Line Model (SSLM); see [7], [8], [9] for example. The SSLM is a random geometric model that offers tools to describe geometric features of access networks and

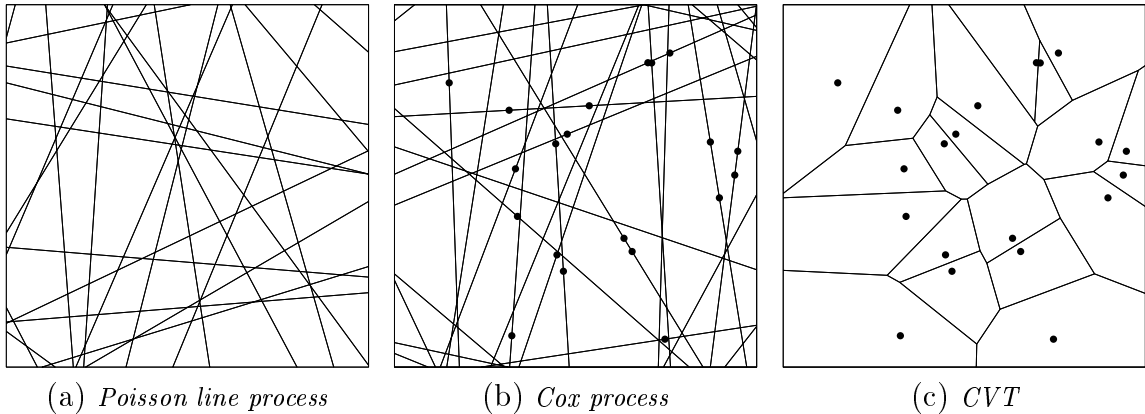


Fig. 1: Poisson line process and Cox–Voronoi tessellation

that allows for stochastic econometrical analysis, like the analysis of connection costs.

The modelling framework of the SSLM can be subdivided into the network geometry model, the network component model, and the network topology model. The network geometry model represents the cable trench system, typically located along the urban infrastructure system, and in the SSLM modelled by random tessellations. Subsequently the network component model places technical network components along the cable trenches according to independent (Poisson) point processes on lines or in the plane. Finally the components are connected with respect to the network topology model.

Methods for an optimal choice of the geometry model with respect to given data can be found in [8]. In [9] an algorithm was introduced in order to simulate typical Cox–Voronoi cells based on linear Poisson processes on random lines; see Fig. 1. In our contribution, this algorithm, together with other techniques, is used to investigate two–level hierarchical models, i.e. models of two different components where the lower–level component is connected to its closest higher–level component, based on Poisson line tessellations. Efficient computation and simulation techniques for network characteristics like mean shortest path length and mean subscriber line length are shown. These network characteristics are key–ingredients to an efficient cost analysis. Notice that Poisson line tessellations are chosen as geometry model since earlier investigations showed that, for a lot of real data situations, they can represent a suitable model for the urban infrastructure. We explain methods which allow for these characteristics to be computed without simulating the locations of lower–level components, thereby enhancing simulation speed enormously. In particular, instead of performing large–scale computations of shortest path lengths and subscriber line lengths, respectively, for each lower–level component individually, we first use an ergodicity argument by which these large–scale computations can be reduced to the computation of a single expectation value with respect to the so–called Palm probability measure induced by the point process of lower–level components. Then, we apply Neveu’s exchange formula for Palm expectations of stationary marked point processes. This allows us to pass to expectations with respect to the Palm probability measure induced by the point process of higher–level components, which are computationally easier to handle. Finally, we compute the latter expectations by partitioning the underlying line system and by applying inner Voronoi tessellations with respect to the edges of the cells formed by the Poisson line process. An extended version of this contribution is given in the paper [10].

All implementations that have been done for the computation and the simulation of

network characteristics and corresponding models are integrated in the GeoStoch library. This JAVA-based library comprises software tools designed to analyze data with methods from stochastic geometry; see [11] and <http://www.geostoch.de>.

2 Stochastic modelling of telecommunication access networks

In the following we regard two-level hierarchical models, i.e., two different equipment types are placed along the infrastructure system. More precisely, we start by considering a Poisson line process, which is intended to model the underlying road system. Given a realization of such an underlying line system we independently generate either two (marked) point processes on each line, which can be seen as spatial point processes concentrated on the system of lines, or we generate one of the two point processes within the cells formed by the lines of the underlying line system.

2.1 Network geometry and higher-level components

As a model for the underlying infrastructure system, or in other words the network geometry, a Poisson line tessellation is chosen which is induced by a stationary and isotropic Poisson line process X_ℓ with intensity γ . The higher-level components are placed on the lines of this line system, in agreement with the rules defined by the SSLM. Furthermore, the locations of higher-order components are assumed to form a (non-marked) stationary point process $X_H = \{X_n\}_{n \geq 1}$ in \mathbb{R}^2 with intensity λ_H .

Later on in Section 5, we will assume that X_H is a doubly stochastic Poisson process whose (random) intensity measure is concentrated on the lines of the underlying Poisson line process X_ℓ . However, for the purposes of Sections 3 and 4, this assumption is unnecessarily strong. Thus, for the moment, we only assume that X_H satisfies the following conditions. Given X_ℓ , consider independent stationary and ergodic (linear) point processes on each line of X_ℓ and let X_H be the superposition of these point processes. Their (linear) intensity λ_1 , measured along the lines of X_ℓ , is connected to the (full-dimensional) intensity λ_H via $\lambda_H = \lambda_1 \gamma$.

Furthermore, suppose that each location X_n of a higher-level component has an influence zone $\Xi(X_n)$ and that the sequence $\{\Xi(X_n)\}_{n \geq 1}$ forms a Voronoi tessellation induced by X_H ; see Fig. 1(c).

Theorem 2.1 *Let Ξ^* denote the typical cell of the Voronoi tessellation $\{\Xi(X_n)\}_{n \geq 1}$ induced by the stationary point process $X_H = \{X_n\}_{n \geq 1}$ of higher-level components. Then,*

$$\lambda_1 = \frac{1}{\mathbb{E}_{X_H} \nu_1(L(\Xi^*))}, \quad (2.1)$$

where \mathbb{E}_{X_H} denotes expectation with respect to the Palm probability measure $\mathbb{P}_{X_H}^*$ and where $L(\Xi^*)$ denotes the (Palm) line system within the typical cell Ξ^* .

2.2 Lower-level components and shortest paths

With respect to the placement of lower-level components two different scenarios are regarded. In a first scenario, given X_ℓ , the lower-level components are placed according to independent Poisson point processes with (linear) intensity λ_2 on the lines of the Poisson line process X_ℓ ; see Fig. 2(a). Then, the union $\{\tilde{X}_n\}_{n \geq 1}$ of all locations \tilde{X}_n of lower-level components forms a stationary (doubly stochastic Poisson) point process in \mathbb{R}^2 whose

(planar) intensity is denoted by λ_L . Notice that $\lambda_L = \lambda_2\gamma$. To exclude trivial cases, we always assume in this paper that $0 < \lambda_H, \lambda_L < \infty$.

Let $N(\tilde{X}_n)$ denote the location of the nearest (in the Euclidean sense) higher-level component of \tilde{X}_n and let $P(\tilde{X}_n, N(\tilde{X}_n))$ be the shortest path from \tilde{X}_n to $N(\tilde{X}_n)$ along the edges of the graph induced by the Poisson line process X_ℓ . By $c(P(\tilde{X}_n, N(\tilde{X}_n)))$ we denote the length of the path $P(\tilde{X}_n, N(\tilde{X}_n))$.

An important network characteristic of special interest is the mean shortest path length, i.e., the average distance with respect to the underlying graph structure from the lower-level components to their nearest (in the Euclidean sense) higher-level components. In order to analyze this characteristic, each location \tilde{X}_n of the lower-level components is associated with the mark $c(P(\tilde{X}_n, N(\tilde{X}_n))) > 0$. This leads to the stationary marked point process

$$X_L = \{[\tilde{X}_n, c(P(\tilde{X}_n, N(\tilde{X}_n)))]\}_{n \geq 1}, \quad (2.2)$$

whose mark space is the non-negative x -axis $[0, \infty]$.

In a second scenario, the lower-level components are not placed on the edges, but into the cells formed by the Poisson line process X_ℓ , according to an independent (stationary) Poisson point process $\{X'_n\}_{n \geq 1}$ in \mathbb{R}^2 with (planar) intensity λ_L . Afterwards, for each n , the location X'_n of the n th lower-level component is connected with the location $N(X'_n)$ of its nearest (in the Euclidean sense) higher-level component. This is done in the following way.

Let $\Xi_n = \Xi(N(X'_n))$ be the Voronoi cell of $N(X'_n)$ and let $L(\Xi_n)$ denote the restriction of the Poisson line process X_ℓ to Ξ_n . Then, the location X'_n is first connected to its nearest point of the line system $L(\Xi_n)$; see Fig. 2(b). This “projection point” is denoted by X''_n . We are interested in the mean subscriber line length, representing the average shortest distance of the projected points X''_n on the lines to the locations $N(X'_n)$ of their higher-order components, with respect to the underlying graph structure induced the Poisson line process X_ℓ . Again, these distances can be expressed via the marks $c(P(X'_n, N(X'_n)))$, attached to the locations X'_n of lower-level components. However, in this second placement scenario, one can split up the marks according to

$$c(P(X'_n, N(X'_n))) = c'(X'_n, X''_n) + c(P(X''_n, N(X'_n))), \quad (2.3)$$

where $c'(X'_n, X''_n)$ is the cost value of the “edge” with respective endpoints X'_n and X''_n . Note that in Section 5, we assume $c'(X'_n, X''_n) = 0$ in order to enhance the clarity of presentation.

3 Mean shortest path length

In this section we investigate the mean shortest path length for the first location scenario of lower-level components described in Section 2.2.

3.1 Simulation methods

At first glance, a natural approach in order to practically analyze the mean shortest path length seems to be the following procedure. First, simulate the network in a (supposedly large) sampling window $W \subset \mathbb{R}^2$, then compute the shortest path length $c(P(\tilde{X}_n, N(\tilde{X}_n)))$ for each location \tilde{X}_n of lower-level components generated in the sampling window, and,

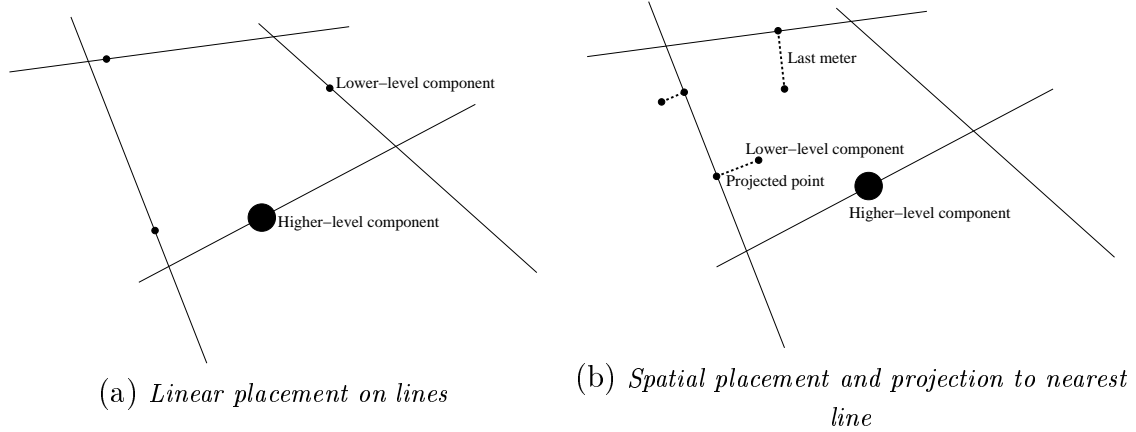


Fig. 2: Two scenarios for the placement of lower-level components

finally compute the average $c_{LH}(W)$ of these shortest path lengths, where

$$c_{LH}(W) = \frac{1}{\#\{n : \tilde{X}_n \in W\}} \sum_{n \geq 1} \mathbb{I}_W(\tilde{X}_n) c(P(\tilde{X}_n, N(\tilde{X}_n))). \quad (3.1)$$

However, it becomes very rapidly clear that this method has some distinct disadvantages. If the sampling window W is too small, the problem of edge-effects is significant. If, on the other hand, W is large, the computational problem arises that a lot of memory and runtime is needed for single simulation runs.

Therefore, we propose an alternative approach by using the Palm probability measure $\mathbb{P}_{X_L}^*$ of the stationary marked point process $X_L = \{[\tilde{X}_n, c(P(\tilde{X}_n, N(\tilde{X}_n)))]\}_{n \geq 1}$, introduced in (2.2). This alternative approach is based on the following asymptotic property of the random variable $c_{LH}(W)$ defined in (3.1). Let $\{W_i\}_{i \geq 1}$ be a so-called averaging sequence of unboundedly increasing sampling windows. Then, by the ergodicity of the stationary marked point process X_L , we have that

$$\lim_{i \rightarrow \infty} c_{LH}(W_i) = c_{LH}^* \quad (3.2)$$

holds with probability 1, where

$$c_{LH}^* = \frac{1}{\lambda_L \nu_2(B)} \mathbb{E} \sum_{n \geq 1} \mathbb{I}_B(\tilde{X}_n) c(P(\tilde{X}_n, N(\tilde{X}_n))) = \mathbb{E}_{X_L} c(P(o, N(o))). \quad (3.3)$$

Recall that the symbol B in (3.3) means an arbitrary (bounded) Borel set $B \in \mathcal{B}(\mathbb{R}^2)$ with $0 < \nu_2(B) < \infty$ and \mathbb{E}_{X_L} denotes expectation with respect to the Palm probability measure $\mathbb{P}_{X_L}^*$.

Thus, motivated by the limit in (3.2), we will compute $c_{LH}^* = \mathbb{E}_{X_L} c(P(o, N(o)))$, which will be much easier than computing the average $c_{LH}(W)$ given in (3.1). Moreover, by Neveu's exchange formula for Palm expectations, we can express c_{LH}^* in an even more favorable way; see Section 3.2.

3.2 Application of Neveu's formula

The following result admits a practically more feasible representation of the expectation $c_{LH}^* = \mathbb{E}_{X_L} c(P(o, N(o)))$ appearing in (3.2) and, in the consequence, a more efficient way to approximately compute the mean shortest path length $c_{LH}(W)$ considered in (3.1).

Theorem 3.1 Consider the point process $X_H = \{X_n\}_{n \geq 1}$ of locations of higher-level components and the (marked) point process $X_L = \{[\tilde{X}_n, c(P(\tilde{X}_n, N(\tilde{X}_n)))]\}_{n \geq 1}$. Then,

$$\mathbb{E}_{X_L} c(P(o, N(o))) = \frac{1}{\mathbb{E}_{X_H} \nu_1(L(\Xi^*))} \mathbb{E}_{X_H} \int_{L(\Xi^*)} c(P(u, o)) du, \quad (3.4)$$

where Ξ^* denotes the typical cell of the Voronoi tessellation induced by X_H and $L(\Xi^*)$ is the (Palm) line system within Ξ^* .

Notice that by Theorem 3.1, we can further simplify the computation of the mean shortest path length $c_{LH}(W)$ considered in (3.1). Namely, instead of computing the expectation $c_{LH}^* = \mathbb{E}_{X_L} c(P(o, N(o)))$ appearing in (3.2), we will estimate the quotient of expectations on the right-hand side of (3.4). For doing so, we just have to simulate the typical serving zone Ξ^* of higher-level components, together with their corresponding (typical) line system, where $L(\Xi^*)$ denotes this line system restricted to Ξ^* .

We also remark that the expression for $\mathbb{E}_{X_L} c(P(o, N(o)))$ given in (3.4) can be alternatively written in the form

$$\mathbb{E}_{X_L} c(P(o, N(o))) = \lambda_1 \mathbb{E}_{X_H} \int_{L(\Xi^*)} c(P(u, o)) du, \quad (3.5)$$

which immediately follows from Theorems 2.1 and 3.1. This shows in particular that the expectation $\mathbb{E}_{X_L} c(P(o, N(o)))$ does actually not depend on λ_2 .

3.3 Computational algorithm

In order to get an estimator \hat{c}_{LH} for c_{LH}^* , we use the expression (3.4) derived in Theorem 3.1. The idea is to simulate the typical Voronoi cell Ξ^* , and the (typical) line system $L(\Xi^*)$, a certain number of times, k say. Furthermore, we partition the line system $L(\Xi_i^*)$ in Ξ_i^* for $i = 1, \dots, k$ into its line segments $E_i = \{S_i^{(1)}, S_i^{(2)}, \dots, S_i^{(M_i)}\}$, where M_i is the total number of line segments in Ξ_i^* for $1 \leq i \leq k$. Notice that the line which contains the origin is subdivided into two segments; see Fig. 3(a).

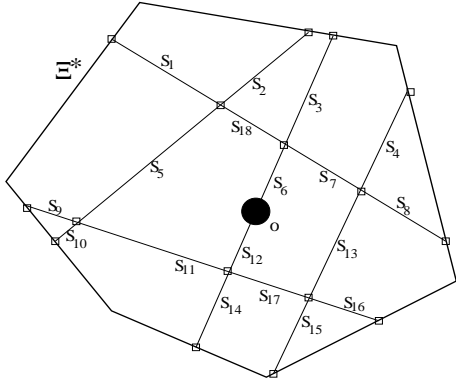
Hence, taking classical sample means, we get that $\lim_{k \rightarrow \infty} \hat{c}_{LH}(k) = c_{LH}^*$ with probability 1, where

$$\hat{c}_{LH}(k) = \frac{1}{\sum_{i=1}^k \nu_1(L(\Xi_i^*))} \sum_{i=1}^k \sum_{j=1}^{M_i} \int_{S_i^{(j)}} c(P(u, o)) du. \quad (3.6)$$

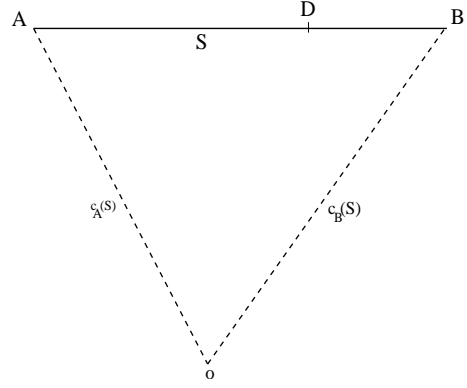
Alternatively, if the intensity λ_1 is known, we can use the relationship (3.5) in order to get still another estimator $\check{c}_{LH}(k)$ for c_{LH}^* , where

$$\check{c}_{LH}(k) = \lambda_1 \frac{1}{k} \sum_{i=1}^k \sum_{j=1}^{M_i} \int_{S_i^{(j)}} c(P(u, o)) du. \quad (3.7)$$

In both cases, it remains to know how the integrals on the right-hand sides of (3.6) and (3.7), respectively, can be computed. This is shown in the following theorem, where some additional assumptions will be made on the cost function $c : E \rightarrow [0, \infty)$.



(a) Partitioning of $L(\Xi_i^*)$ into segments



(b) Mean shortest path length for single segment

Fig. 3: Partitioning and weighted mean shortest path length

Theorem 3.2 Suppose that the values $c(e)$ of the cost function $c : E \rightarrow [0, \infty)$ only depend on the lengths of the edges $e \in E$ and that $c(e)$ is monotonously increasing with respect to the length of e , where $c(e) = 0$ if $\nu_1(e) = 0$. Let $S = S(A, B)$ be a line segment with respective endpoints A and B , and let $\delta_S = c(P(B, o)) - c(P(A, o))$. Then,

$$c(P(A, B)) \geq |\delta_S|. \quad (3.8)$$

Moreover, there exists a point $D \in S$ such that

$$c(P(A, o)) + c(P(D, A)) = c(P(B, o)) + c(P(D, B)) \quad (3.9)$$

and

$$\begin{aligned} \int_S c(P(u, o)) du &= c(P(A, o))\nu_1(D - A) + \int_D^A c(P(A, u)) du \\ &+ c(P(B, o))\nu_1(D - B) + \int_D^B c(P(B, u)) du. \end{aligned} \quad (3.10)$$

Corollary 3.1 If $c(S)$ is the length of the segment $S = S(A, B)$, i.e. $c(S) = \nu_1(S)$, then

$$\int_S c(P(u, o)) du = f(\nu_1(S); c(P(A(S), o)), c(P(B(S), o))), \quad (3.11)$$

where

$$f(x; \theta_1, \theta_2) = \frac{1}{4}x^2 + \frac{1}{2}(\theta_1 + \theta_2)x - \frac{1}{4}(\theta_2 - \theta_1)^2. \quad (3.12)$$

If $c(e) = \nu_1(e)$ for any $e \in E_i$ for $i = 1, \dots, k$ and $k \geq 1$ then by Corollary 3.1, we immediately get the following final expressions for the estimators $\hat{c}_{LH}(k)$ and $\check{c}_{LH}(k)$.

Corollary 3.2 For each $k \geq 1$ let $E_i = \{S_i^{(j)}\}_{j=1}^{M_i}$ be the partition of the line system $L(\Xi_i^*)$ restricted to the i th typical cell Ξ_i^* for $i = 1, \dots, k$ and let $A_i^{(j)}$ and $B_i^{(j)}$, respectively, denote the endpoints of the segment S_i^j . Then,

$$\hat{c}_{LH}(k) = \frac{1}{\sum_{i=1}^k \nu_1(L(\Xi_i^*))} \sum_{i=1}^k \sum_{j=1}^{M_i} f(\nu_1(S_i^{(j)}); c(P(A_i^{(j)}), o), c(P(B_i^{(j)}), o)) \quad (3.13)$$

and

$$\check{c}_{LH}(k) = \frac{\lambda_1}{k} \sum_{i=1}^k \sum_{j=1}^{M_i} f(\nu_1(S_i^{(j)}); c(P(A_i^{(j)}), o), c(P(B_i^{(j)}), o)), \quad (3.14)$$

where the function f is given in (3.12).

By the representation formulae (3.13) and (3.14), it suffices to compute the path lengths $c(P(A_i^{(j)}), o)$ and $c(P(B_i^{(j)}), o)$ for $j = 1, \dots, M_i$ and $i = 1, \dots, k$ in order to determine the estimators $\widehat{c}_{LH}(k)$ and $\check{c}_{LH}(k)$. This can be done, for example, by applying Dijkstra's algorithm; see Section 5 below.

4 Mean subscriber line length

In this section we consider the case, where the lower-level components are not placed on the edges, but into the cells formed by the Poisson line process X_ℓ , according to an independent (stationary) Poisson point process $\{X'_n\}_{n \geq 1}$ in \mathbb{R}^2 with (planar) intensity λ_L ; see Section 2.2.

Recall that, for each n , the location X'_n of the n th lower-level component is connected with the location $N(X'_n)$ of its nearest (in the Euclidean sense) higher-level component. For this purpose, X'_n is first connected to its nearest point X''_n of the line system $L(\Xi_n)$, where $\Xi_n = \Xi(N(X'_n))$ is the Voronoi cell of $N(X'_n)$ and $L(\Xi_n)$ denotes the restriction of the Poisson line process X_ℓ to Ξ_n .

An interesting characteristic is the so-called mean subscriber line length

$$d_{LH}(W) = \frac{1}{\#\{n : X'_n \in W\}} \sum_{n \geq 1} \mathbb{1}_W(X'_n) c(P(X'_n, N(X'_n))) \quad (4.1)$$

for some sampling window $W \subset \mathbb{R}^2$, where the cost value $c(P(X'_n, N(X'_n)))$ of the shortest path from X'_n to $N(X'_n)$ is given in (2.3).

In order to practically analyze the mean subscriber line length $d_{LH}(W)$, we propose an approach which is analogous to that considered in Section 3, i.e., an approach based on the Palm probability measure $\mathbb{P}_{X'_L}^*$ of the stationary marked point process $X'_L = \{[X'_n, c(X'_n)]\}_{n \geq 1}$, where $c(X'_n) = c(P(X'_n, N(X'_n)))$. Then, by the ergodicity of X'_L , we have that

$$\lim_{i \rightarrow \infty} d_{LH}(W_i) = d_{LH}^* \quad (4.2)$$

holds with probability 1, where $\{W_i\}_{i \geq 1}$ is an averaging sequence of unboundedly increasing sampling windows and

$$d_{LH}^* = \frac{1}{\lambda_L \nu_2(B)} \mathbb{E} \sum_{n \geq 1} \mathbb{1}_B(X'_n) c(P(X'_n, N(X'_n))) = \mathbb{E}_{X'_L} c(P(o, N(o))) \quad (4.3)$$

for some (bounded) Borel set $B \in \mathcal{B}(\mathbb{R}^2)$ with $0 < \nu_2(B) < \infty$.

Furthermore, applying Neveu's exchange formula for Palm expectations, we get the following expression for the expectation $\mathbb{E}_{X'_L} c(P(o, N(o)))$ appearing in (4.3).

Theorem 4.1 *Consider the point process $X_H = \{X_n\}_{n \geq 1}$ of higher-level components and the (marked) point process $X'_L = \{[X'_n, c(P(X'_n, N(X'_n)))]\}_{n \geq 1}$. Then,*

$$\mathbb{E}_{X'_L} c(P(o, N(o))) = \frac{1}{\mathbb{E}_{X_H} \nu_2(\Xi^*)} \mathbb{E}_{X_H} \int_{\Xi^*} c(P(u, o)) du, \quad (4.4)$$

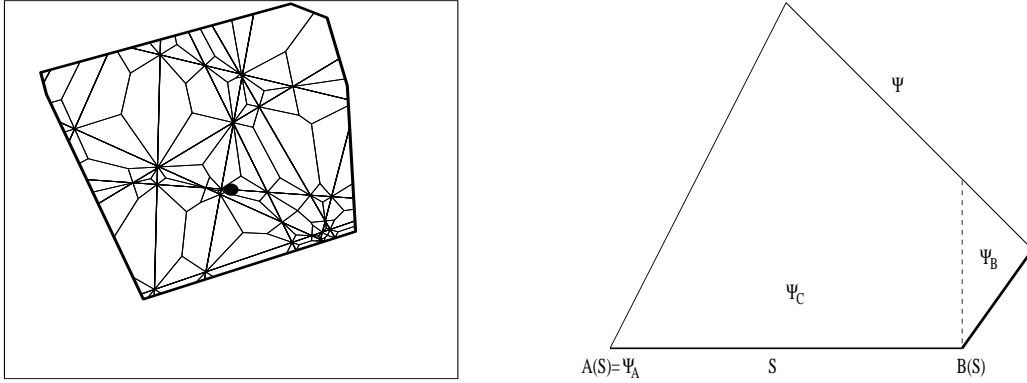


Fig. 4: Computational aspects of \widehat{d}_{LH} : Typical Cox-Voronoi cell with inner Voronoi tessellation (left) and example of inner Voronoi cell (right)

where Ξ^* denotes the typical cell of the Voronoi tessellation induced by X_H .

Using (4.3) and (4.4), we get an estimator \widehat{d}_{LH} for the limit d_{LH}^* considered in (4.2), where $\lim_{k \rightarrow \infty} \widehat{d}_{LH}(k) = d_{LH}^*$ with probability 1, and where

$$\widehat{d}_{LH}(k) = \frac{1}{\sum_{i=1}^k \nu_2(\Xi_i^*)} \sum_{i=1}^k \sum_{j=1}^{K_i} \int_{\Psi_i^{(j)}} c(P(u, o)) du. \quad (4.5)$$

The second summation is done over the (random) number K_i of inner Voronoi cells $\Psi_i^{(j)}$. Fig. 4 provides a graphical explanation of the computation. For further details, it is referred to [10].

5 Numerical analysis

Recall that in this section we assume X_H to be a doubly stochastic Poisson process as pointed out in Section 2.1. Then, the whole model is completely described by the three parameters λ_L , λ_1 and γ . Besides this we assume that $c(S)$ is the length of the segment S , i.e. $c(S) = \nu_1(S)$.

5.1 Scaling properties of CVT

As it has already been explained in [9], with respect to the two remaining parameters λ_1 and γ , a scaling invariance property holds for any fixed value of the quotient $\kappa = \gamma/\lambda_1$. In particular suppose that $\gamma = a\gamma^{(0)}$ and $\lambda_1 = a\lambda_1^{(0)}$ for some $\gamma^{(0)}, \lambda_1^{(0)} > 0$, fixed and $a > 0$. Then, with respect to the typical cell Ξ^* of the corresponding Voronoi tessellation, the expected number of vertices is constant, whereas the expected perimeter and the square root of the expected area of the typical cell grow linearly, proportionally to a^{-1} .

Furthermore, the following scaling property shows that it is possible to provide estimates for the characteristics described in Sections 3 and 4 corresponding to a given parameter pair (γ, λ_1) by using estimates for a different parameter pair having the same quotient κ and by performing a suitable standardization afterwards.

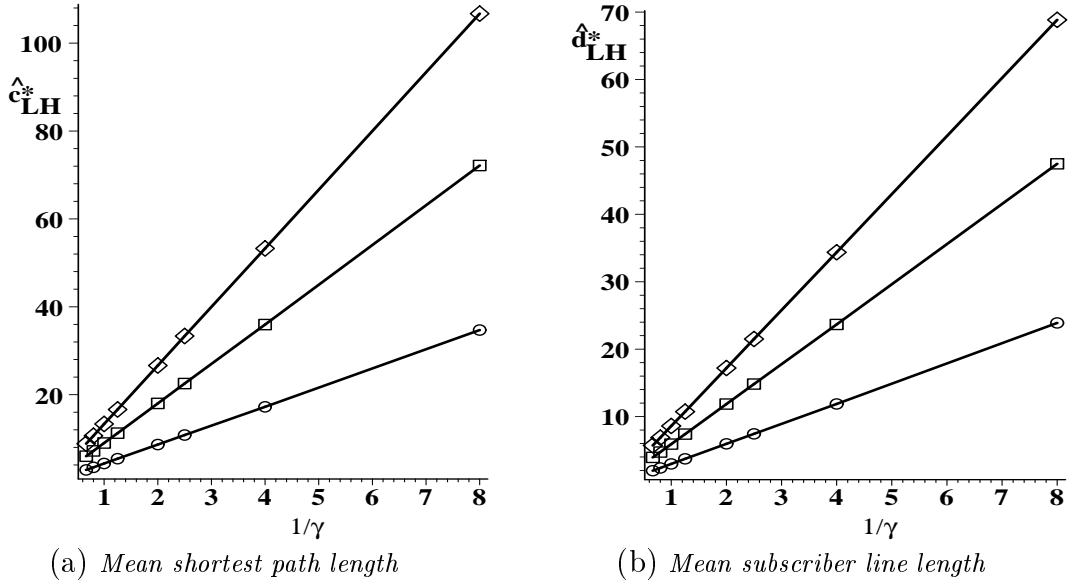


Fig. 5: Network characteristics for $\kappa = 10$ (o), $\kappa = 50$ (+) and $\kappa = 120$ (\diamond)

Theorem 5.1 For any pair (γ, λ_1) of parameters $\gamma, \lambda_1 > 0$, consider the (ergodic) limits $c_{LH}^* = c_{LH}^*(\gamma, \lambda_1)$ and $d_{LH}^* = d_{LH}^*(\gamma, \lambda_1)$ given in (3.2) and (4.2), respectively. Then

$$\gamma^{(1)} c_{LH}^*(\gamma^{(1)}, \lambda_1^{(1)}) = \gamma^{(2)} c_{LH}^*(\gamma^{(2)}, \lambda_1^{(2)}) \quad (5.1)$$

and

$$\gamma^{(1)} d_{LH}^*(\gamma^{(1)}, \lambda_1^{(1)}) = \gamma^{(2)} d_{LH}^*(\gamma^{(2)}, \lambda_1^{(2)}) \quad (5.2)$$

provided that $\gamma^{(1)}/\lambda_1^{(1)} = \gamma^{(2)}/\lambda_1^{(2)}$.

5.2 Numerical results

With regard to the estimation of the mean shortest path length as well as the mean subscriber line length we used $k = 50000$ iterations. Fig. 5 shows a visualization of the scaling invariance effect for the mean shortest path length and the mean subscriber line length. If we take κ to be fixed for different values of γ , then the estimated results for c_{LH}^* as well as for d_{LH}^* are proportional to $1/\gamma$. Therefore the graphs displayed in Fig. 5 for $\kappa = 10$, $\kappa = 50$, and $\kappa = 120$ are linear and should pass through the origin. Of course, the latter property cannot be directly checked since it means that $\gamma \rightarrow \infty$.

A first important observation one can make, is that for the same parameter pair (γ, λ_1) we always have that $c_{LH}^* > d_{LH}^*$. This observation might be explained by the fact that the cells of the Cox–Voronoi tessellation of the upper-level components are convex polygons, hence if each point on the underlying line system is weighted by the distance measure of the points in the cell projected to it, points lying close to the center of the cell get a larger weight than these near the edge. With regard to the estimation of c_{LH}^* , these weights are always constant. Therefore, we have that the mean shortest path length is larger than the mean subscriber line length for the same pair of parameters.

If κ increases, the quotient c_{LH}^*/d_{LH}^* also slightly increases, meaning that in this case the mean shortest path length becomes larger in relation to the mean subscriber line length.

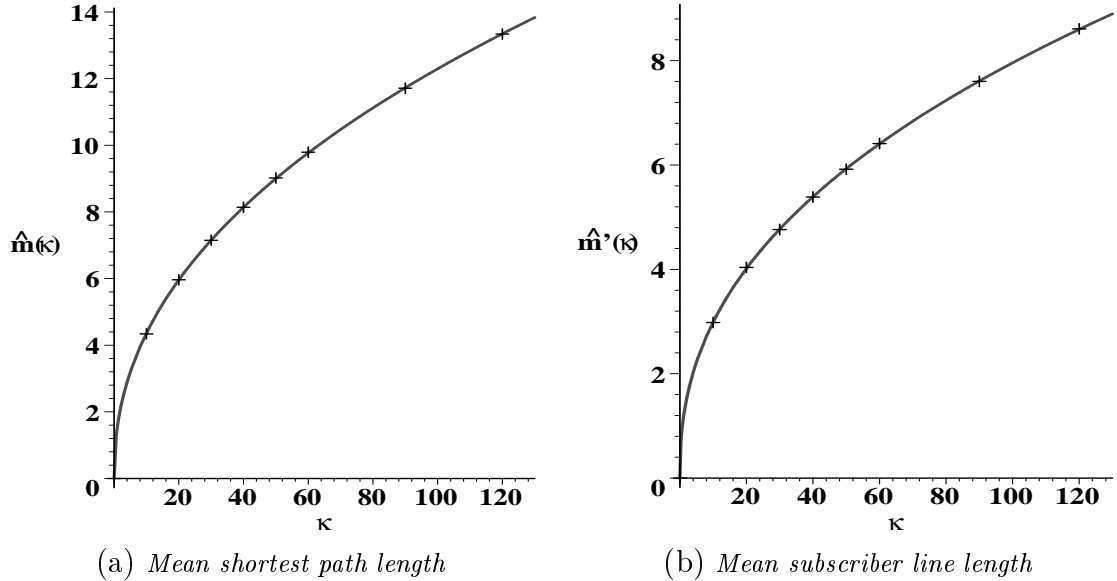


Fig. 6: Estimates for $m(\kappa)$ and $m'(\kappa)$ for different κ and the fitted function

Another interesting observation is that the values of both characteristics seem to increase for increasing κ . Obviously this is due to the fact that the expected area $\mathbb{E}\nu_2(\Xi^*)$ of the typical cell Ξ^* of the Cox–Voronoi tessellation also increases.

Recall that by Theorem 5.1 we have

$$c_{LH}^*(\gamma, \lambda_1) = m(\kappa) \gamma^{-1} \quad \text{and} \quad d_{LH}^*(\gamma, \lambda_1) = m'(\kappa) \gamma^{-1}, \quad (5.3)$$

where $m(\kappa)$ and $m'(\kappa)$ are constants depending only on the quotient $\kappa = \gamma/\lambda_1$. If we return to the graphs displayed in Fig. 5, we can obtain the estimates $\hat{m}(\kappa)$ and $\hat{m}'(\kappa)$ for the slopes $m(\kappa)$ and $m'(\kappa)$ of the lines for κ constant and $1/\gamma$ variable.

The knowledge of $\hat{m}(\kappa)$ and $\hat{m}'(\kappa)$ thereby leads to the possibility of estimating the mean shortest path length and the mean subscriber line length without having to do simulations for any given parameter pair (γ, λ_1) , since then, only these parameter values need to be plugged into the formulas in (5.3) to obtain the estimates for c_{LH}^* and d_{LH}^* , respectively. Computationally these slopes are estimated for certain discrete values of κ and subsequently a function is fitted using the measurement points. Fig. 6 displays some values of estimated slopes as well as a fitted function. Regarding the estimated values we used

$$m(\kappa) = a\kappa^b \quad \text{and} \quad m'(\kappa) = a'\kappa^{b'},$$

where $a, a' \in \mathbb{R}$ and $b, b' \in (0, 1]$. Using the least squares method we obtained $a = 1.5477$, $b = 0.450$ and $a' = 1.1242$, $b' = 0.425$.

Acknowledgement This research was supported by France Télécom R&D through research grant No. 42 36 68 97. The authors are grateful to Michael Rösch for his help in performing the simulations, which lead to the numerical results.

References

- [1] Baccelli, F. and B. Blaszczyzyn, B.: On a coverage process ranging from the Boolean model to the Poisson–Voronoi tessellation. *Advances in Applied Probability* **33** (2001), 293–323.

- [2] Baccelli, F., Gloaguen, C. and Zuyev, S.: Superposition of Planar Voronoi Tessellations. *Communications in Statistics, Series Stochastic Models* **16** (2002), 69–98.
- [3] Baccelli, F., Klein, M., Lebourges, M. and Zuyev, S.: Géométrie aléatoire et architecture de réseaux. *Annales des Télécommunication* **51** (1996), 158–179.
- [4] Baccelli, F., Kofman, D., and Rougier, J.L.: Self organizing hierarchical multicast trees and their optimization. *Proceedings of IEEE Infocom '99*, IEEE Computer Society Press, New York 1999, 1081–1089.
- [5] Baccelli, B. and Zuyev, S.: Poisson-Voronoi spanning trees with applications to the optimization of communication networks. *Operations Research* **47** (1996), 619–631.
- [6] Błaszczyszyn, B. and Schott, R.: Approximations of functionals of some modulated Poisson–Voronoi tessellations with applications to modeling of communication networks. *Japan Journal of Industrial and Applied Mathematics*, **22**(2) (2005), to appear.
- [7] Gloaguen, G., Coupé, P., Maier, R. and Schmidt, V.: Stochastic modelling of urban access networks. In *Proc. 10th Internat. Telecommun. Network Strategy Planning Symp.* (Munich, June 2002), VDE, Berlin 2002, 99–104.
- [8] Gloaguen, G., Fleischer, F., Schmidt, H. and Schmidt, V.: Fitting of stochastic telecommunication network models, via distance measures and Monte-Carlo tests. *Telecommunication Systems* (2006), to appear.
- [9] Gloaguen, G., Fleischer, F., Schmidt, H. and Schmidt, V.: Simulation of typical Cox-Voronoi cells with a special regard to implementation tests. *Mathematical Methods of Operations Research* **62**(3) (2005), 84–95.
- [10] Gloaguen, C., Fleischer, F., Schmidt, H. and Schmidt, V.: Analysis of shortest paths and subscriber line lengths in telecommunication access networks. *Networks and Spatial Economics* (2006), submitted.
- [11] Mayer, J., Schmidt, V. and Schweiggert, F.: A unified simulation framework for spatial stochastic models. *Simulation Modelling Practice and Theory* **12** (2004), 307–326.
- [12] Schneider, R. and Weil, W.: *Stochastische Geometrie*. Teubner, Stuttgart 2000.
- [13] Stoyan D., Kendall W.S. and Mecke, J.: *Stochastic Geometry and its Applications*. 2nd ed., J. Wiley & Sons, Chichester 1995.
- [14] Tchoumatchenko, K. and Zuyev, S.: Aggregate and fractal tessellations. *Probability Theory Related Fields* **121** (2001), 198–218.